Materials Science and Engineering A 526 (2009) 171–176

Contents lists available at ScienceDirect

Materials Science and Engineering A

journal homepage: www.elsevier.com/locate/msea

Influence of constituents on the ductile fracture of Al–Cu–Mg alloys: Modulated by the aging treatment

G.J. Zhang[a,b], R.H. Wang[a,b], S.P. Yuan[b], G. Liu[b,*], S. Scudino[c], J. Sun[b,*], K.H. Chen[d]

[a] School of Material Science & Engineering, Xi'an University of Technology, Xi'an, 710049, China
[b] State Key Laboratory for Mechanical Behavior of Materials, School of Material Science & Engineering, Xi'an Jiaotong University, XianNing West Road 28, Xi'an, 710049, China
[c] IFW Dresden, Institut für Komplexe Materialien, Postfach 27 01 16, D-01171 Dresden, Germany
[d] State Key Laboratory for Powder Metallurgy, The University of Southern Central China, Changsha, 410083, China

ARTICLE INFO

Article history:
Received 26 November 2008
Received in revised form 9 July 2009
Accepted 19 August 2009

Keywords:
Aluminum alloys
Ductile fracture
Aging treatment
Coupling effect
Second phase particles

ABSTRACT

Two different solution treatments and following aging treatment with a series of aging time were respectively applied to Al–Cu–Mg alloys to investigate the coupling effect of constituents and precipitates on the ductile fracture of the heat-treatable aluminum alloys. Ductility and fracture toughness were measured and their dependence on the constituents was clearly shown to be controllable by aging treatment. A multiscale fracture model was used to quantitatively explain the aging-modulated influence of constituents on ductile fracture.

1. Introduction

Heat-treatable aluminum alloys have found extensive practical applications in the aircraft industry related fields and the research on their ductile fracture have been actively carried out. Attention has been generally paid on the relationship between fracture behavior and microstructure of the heat-treatable aluminum alloys [1–3]. Because the microstructure of the heat-treatable aluminum alloys is closely dependent on the heat treatments (including three-step solution, quenching and aging), it is possible to artificially control the ductile fracture of aluminum alloys by tailoring the heat treatments, based on the good understanding and modeling of the technology–microstructure–property relationships in heat-treatable aluminum alloys [1,2].

Previous investigations [e.g. [1]] have shown that, besides the grain size and the grain boundary, other important metallurgy factors that significantly affect the ductile fracture of aluminum alloys are second phase particles inherently contained in the alloys, including large Fe-, Cu-, and Si-rich inclusions (about 1–10 μm in diameter), intermediate Cr-, Mn-, or Zr-rich dispersoids (about 0.05–0.5 μm in diameter), and small precipitates (nanometer size) [1–3]. The large particles, defined as constituents, are brittle in nature and are usually the primary void/crack initiators or the preferential crack propagation path [1]. As a result, the influence of the constituents on the ductile fracture of aluminum alloys has aroused extensive attention. Some classic expressions have been proposed [1,2,4,5] to relate the ductility (the strain to fracture ε_f) and fracture toughness (K_{IC}) to the constituents directly. For example, K_{IC} was given [1] as

$$K_{IC} = \left[4\sigma_y E(\pi/6)^{1/3} d_c\right]^{1/2} f_c^{-1/6} \propto f_c^{-1/6}, \quad (1)$$

where d_c and f_c are the radius and volume fraction of the constituents, respectively, σ_y the yield strength, and E the elastic modulus of the Al alloys. On the other hand, ε_f was related to f_c by [4]

$$\varepsilon_f = \frac{1}{C}\ln\left(\sqrt{\frac{\pi}{6f_c}} - \sqrt{\frac{2}{3}} + \varepsilon_n\right), \quad (2)$$

where C is a factor of about 1.5 that is used to account for the faster extension rate of voids as compared with the matrix before the critical condition for instability is reached, and ε_n is the critical strain for nucleating voids around the constituents. These expressions, although reflecting the relationship between the constituents and the ductile fracture properties to some degree, do not consider the influence of other types of second phase particles, i.e., dispersoid

* Corresponding authors. Fax: +86 29 82663453.
E-mail addresses: lgsammer@mail.xjtu.edu.cn (G. Liu), junsun@mail.xjtu.edu.cn (J. Sun).

0921-5093/$ – see front matter © 2009 Elsevier B.V. All rights reserved.
doi:10.1016/j.msea.2009.08.042

and precipitate, which, in practice, affect the fracture process of aluminum alloys. Decohesion of dispersoids will induces the formation of void sheet, which will truncate the primary voids and thus preclude a large strain accumulation [6,7]. The dislocation pinning at precipitates will cause remarkable stress concentration, resulting in a similar decrease in ductility and fracture toughness [1,8]. The influence of precipitates can be easily reflected by the aging dependent fracture behavior of the heat-treatable aluminum alloys [9–11].

Most recently, a multiscale fracture model [12,13] has been developed to describe both the separate and coupled effects of the three classes of second phase particles on the ductile fracture of aged aluminum alloys by using a unified expression, where the parameters (e.g., volume fraction, size, and aspect ratio) of all the particles are taken into account. From this model, the ductility and fracture toughness of aged aluminum alloys can be related not only to the constituents but also to the dispersoids and the precipitates. Because the volume fraction of precipitates increases concomitantly with reducing the constituents, the multiscale fracture model was further used [14,15] to analyze a coupling effect of the trade-off in volume fraction between the constituents and the precipitates, which could be obtained by adjusting the solution treatment. Calculations were found to be in good agreement with the experimental results [14,15]. However, the comparison between the calculations and the experimental ones were made exclusively at peak-aging condition, which means that the aging time is not the same for the alloys that contain different constituents/precipitates. This, although simplifying the comparison, cannot yield more universal results. Accordingly, in the present work, the same aging time is used for samples with different solution treatments. By this, the coupling effect of the constituents and the precipitates can be clearly revealed from the aging-modulated influence of constituents on the ductility and fracture toughness of a heat-treatable Al–Cu–Mg alloy.

2. Experimental

The Al–Cu–Mg plate and extruded rod used in present work has a chemical composition of 4.62% Cu, 0.65% Mg, 0.22% Mn, 0.08% Si, 0.1% Fe, 0.1% Zn, and balance Al (in wt.%). Enhanced solution treatment followed by fast quenching (EF) and traditional solution treatment followed by fast quenching (TF) were respectively applied to this alloy. The EF treatment was used to dissolve soluble constituents and to cause a concomitant increase of the amount of precipitates. TF was done at 766 K for 2 h followed by quenching into cold (10 °C) water. Enhanced solution treatment was done at 766 K for 2 h followed by holding at an increasing treatment temperature up to 776 K with a rate of 4 K/h. The EF- and TF-treated samples were subsequently aged at 483 K from 0.1 to 10 h. The maximum error of all the temperature measurements in present experiments was ±1 K. The yield strength σ_y, the strain to fracture ε_f, and fracture toughness K_{IC} were measured for the as-quenched samples as well as for the samples aged at 1, 3, and 6 h. σ_y and ε_f were measured by using smooth dog-bone-shaped tensile specimens with a gauge size of 6 mm in diameter and 40 mm in length. All the specimens had an axis along the longitudinal direction. The tensile test was performed at a constant strain rate of $5 \times 10^{-4}\ s^{-1}$ with the load direction parallel to the specimen axis. The yield stress was determined as the 0.2% offset and the strain to fracture was determined as $\varepsilon_f = \ln(A_0/A_f)$, where A_0 is the initial area and A_f is the area at fracture of the specimens.

The fracture toughness was characterized by using compact tension specimens and the *R* curve method. The specimens, with the fracture plane normal to the longitudinal direction of the plate and an expected direction of crack propagation coincident with the width direction of the plate, have been measured with applied loading along with the longitudinal direction. All the specimens had a same size of 62.5 mm in width and 6.25 mm in thickness. Prior to the fracture toughness experiment, the specimens were fatigue cracked at a constant stress ratio ($R = K_{min}/K_{max}$) of 0.1 and under decreasing stress intensity condition. Strictly conforming to ASTM E561, the *R*-curve characterization of fracture toughness was performed on a servohydraulic Instron-type testing machine by using potential-drop method to measure crack length. The crack growth resistance curve was recorded and the plane strain fracture toughness was determined at fracture initiation. All the geometry requirements for plane-strain constraint were met and the obtained plane strain fracture toughness from *R*-curve has been experimentally found to be approximately equal to that determined according to ASTM E399.

The size and volume fraction of the constituents and dispersoids were quantitatively measured by using scanning electron microscopy (SEM) and transmission electron microscopy (TEM), respectively [14,15]. Thin foils for TEM characterization were prepared by mechanical thinning with SiC paper to 100 μm, followed by electropolishing with an applied potential of 15 V in a 3:1 methanol–nitric solution cooled to −25 °C. The foils were rinsed

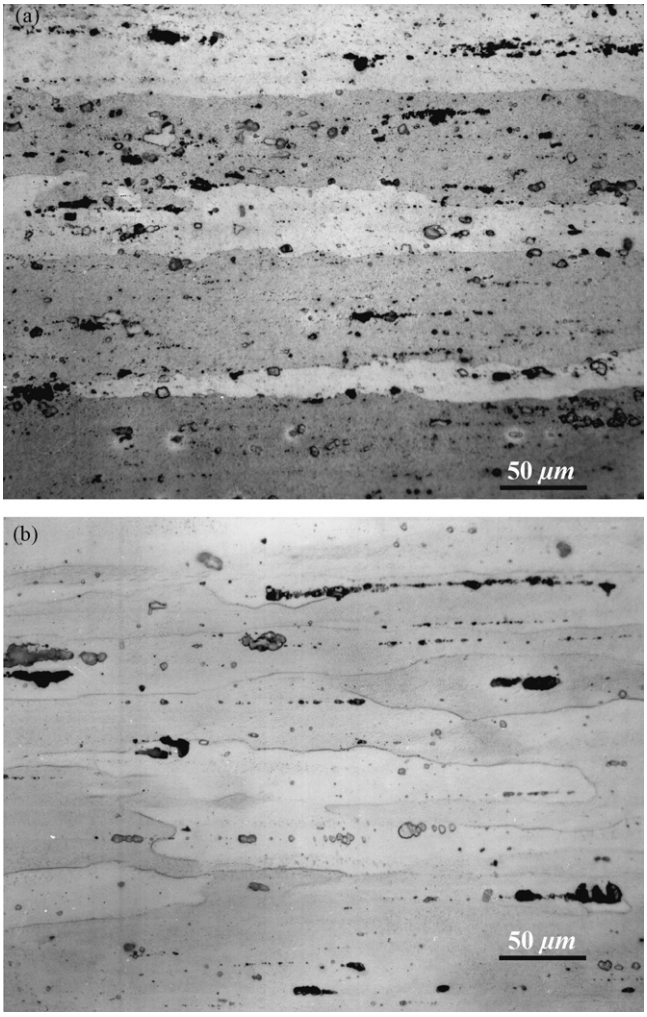

Fig. 1. SEM micrographs of the TF-treated sample (a) and EF-treated sample (b). TF includes solution treatment at 766 K for 2 h followed by aging at 483 K, and EF includes solution treatment at 766 K for 2 h followed by holding at an increasing treatment temperature up to 776 K with a rate of 4 K/h and subsequently by aging at 483 K. Comparison shows that the EF-treated sample contains less constituents than the TF-treated sample.

twice in methanol, dried, and examined immediately in a JEOL Ltd. JEM-200CX TEM at 100 Kv. The size and the volume fraction of the precipitates were determined from at least 600 random precipitates seen edge-on [16].

3. Results and discussions

3.1. Microstructures

Typical micrographs of EF- and TF-treated samples are shown in Fig. 1. Statistical analyses reveal that the grain sizes of the two kinds of samples are almost the same. However, the EF-treated sample contains much less constituents than the TF-treated counterpart. Quantitatively, the volume fractions of the constituents in the EF- and TF-treated sample is about 2.55% and 4.83%, respectively. The enhanced solution treatment dissolves most of the small constituents, leaving the large constituents unaffected. The constituents in the EF-treated sample have an average radius of about 4.32 μm, which is larger than that in TF-treated sample (about 3.91 μm).

The constituents in aluminum alloys can be divided into two types. One type is resulted from the presence of impurities and excessive alloying elements, and the other contains alloying element as well but is resulted from the nonequilibrium solidification due to the lower solvus limit of alloying element in aluminum. In principle, the latter constituents are soluble and could be dissolved into the solid solution reversibly through solution treatment. It is then possible to solubilize these soluble constituents with applying a following enhanced solution treatment. As mentioned above, the enhanced solution treatment in EF is actually a stepped solution treatment, where the solution treatment will be performed at a gradually elevated temperature with time. In comparison, the traditional solution treatment in TF is usually performed at a stationary temperature and, in order to avoid the presence of transient liquid phase, the stationary temperature will be much limited with not exceeding the melting point of multiphase eutectic. Since each of eutectic phases dissolves into matrix in certain sequence during solution treatment, eutectic temperature will be elevated with the complete solution of one of eutectic phases. This indicates that the upper limit temperature for solution will gradually increase during the treatment and so the application of traditional solution treatment with stationary lower temperature could not dissolve more soluble constituents as possible. In contrast, the application of stepped solution treatment with gradual increase in temperature could both avoid exceeding the eutectic melting and realize the complete solution of dissolvable constituents. So the enhanced solution treatment or stepped solution treatment can be employed to dissolve most of the small constituents.

During the following aging treatment, the nucleation and growth of the precipitates in the EF-treated sample is faster, because more solute atoms have been dissolved in the matrix. Fig. 2 shows the typical TEM images of the plate-shaped precipitates in both the EF- and the TF-treated samples aged to 3 and 6 h, revealing a larger amount of precipitates in the EF-treated sample. The size and volume fraction of the precipitates have been measured and plotted in Fig. 3 as a function of aging time. In the under-aged stage, the average radius (r_p) of the plate-shaped precipitates is roughly proportional to the square root of aging time (t), i.e.,

$$r_p = k\sqrt{t}, \tag{3}$$

where k is a growth constant that is related mainly to the supersaturation and the diffusion coefficient of solute atom in the Al matrix. By fitting the experimental results to Eq. (3), it was found that k is 0.62 nm $s^{-1/2}$ for the TF-treated sample and 0.91 nm $s^{-1/2}$ for the EF-treated sample. In the over-aged stage, however, the growth rate of the precipitates is depressed because excessive solute atoms have been consumed and the further growth of precipitates will proceed via Ostwald ripening. The evolution of precipitate content (f_p) with aging time follows a similar Avrami type relationship in both the two kinds of alloys,

$$f_p = f_{\max}\left[1 - \exp(-t/t_0)^m\right], \tag{4}$$

where the maximum volume fraction of precipitates $f_{\max}$, precipitation constant t_0, and dimensionless exponent m, are experimentally

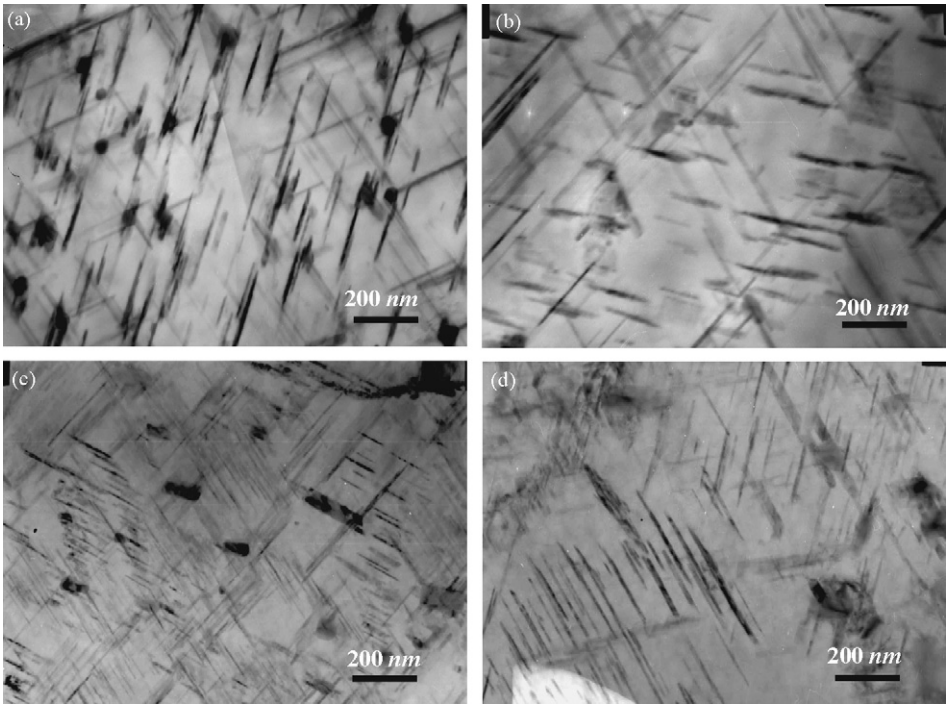

Fig. 2. Typical TEM image showing: (a) and (b) precipitates in the TF-treated and (c) and (d) precipitates in the EF-treated samples. The aging time was 3 h for the images (a) and (c) and 6 h for the images (b) and (d).

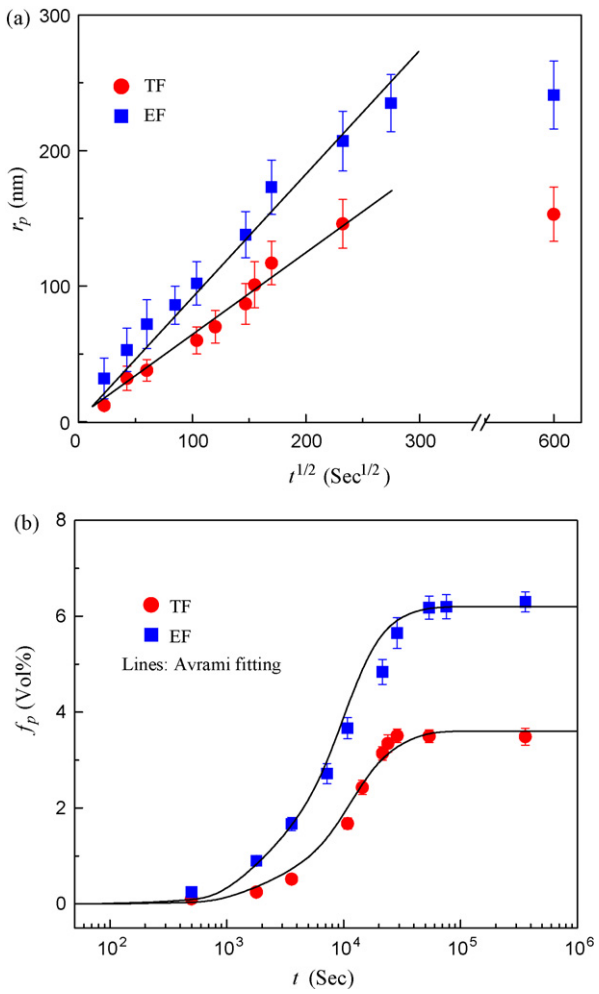

Fig. 3. Size evolution (a) and volume fraction evolution (b) of the precipitates in both TF-treated and EF-treated samples. Dots are experimental results and lines are fitting results.

determined as 3.6 vol.%, 1.25×10^4 s and 1.5 for the TF-treated sample, and 6.2 vol.%, 1.0×10^4 s and 1.5 for the EF-treated sample.

Quantitative analyses indicate that, at a same aging time t, the precipitates in the EF-treated samples have a larger size and more content than those in the TF-treated samples. This is because more solute atoms have been dissolved into the matrix in the EF-treated samples. As a result, the driving force for nucleation and growth of precipitates is greater in this kind of samples. On the other hand, small constituents survived in the TF-treated samples consume more solute atoms. The precipitation in the TF-treated samples is then somewhat limited because of the lack in available solute atoms. At different aging time, however, the precipitates in the long-aged TF-treated samples can have a larger size and more volume fraction than those in the short-aged EF-treated ones. This means that the parameters of precipitates are controllable by experimental design, which will in turn have remarkable effect on the mechanical properties of the alloys.

3.2. Mechanical properties

Due to the evolution of precipitates, the mechanical properties of Al–Cu–Mg alloys vary with aging time. Table 1 lists the variation of σ_y, ε_f and K_{IC} with aging time in both the EF- and the TF-treated samples. For the same aging time, the EF-treated sample always exhibits larger σ_y, ε_f and K_{IC} compared with the TF-treated sample. This is because the EF-treated sample has more strengthening

Table 1
Mechanical properties of the tested samples.

t (h)	EF			TF		
	σ_y (MPa)	ε_f	K_{IC} (MPa m$^{1/2}$)	σ_y (MPa)	ε_f	K_{IC} (MPa m$^{1/2}$)
0	235	0.48	27.4	182	0.34	24.5
1	260	0.41	25.4	200	0.31	23.1
3	306	0.36	24.0	244	0.28	21.4
6	421	0.32	22.5	332	0.24	20.6

precipitates and less constituents. Within the range from $t = 0$ (as-quenched condition) to 6 h (under-aged stage), both the samples show an increase in σ_y but decrease in ε_f and K_{IC} with prolonging the aging time. This indicates that the ductile fracture of present Al–Cu–Mg alloy not only significantly depends on the constituents but also on the aging-induced precipitates.

Fig. 4(a) and (b) shows the dependence of ductility and fracture toughness on the volume fraction of constituents as a function of t. Calculations from Eqs. (2) and (1), respectively, are shown in these figures for comparison (short dot lines). Although Eqs. (2) and (1) give some quantitative description on the relationship between the ductility/fracture toughness and f_c, they cannot account for the influence of precipitates or aging treatment. In the following, the multiscale fracture model will be used to understand the aging-modulated dependence of ductility and fracture toughness on the constituents.

According to the multiscale fracture model [12,13], ε_f and K_{IC} of heat-treatable aluminum alloys can be related to the constituents,

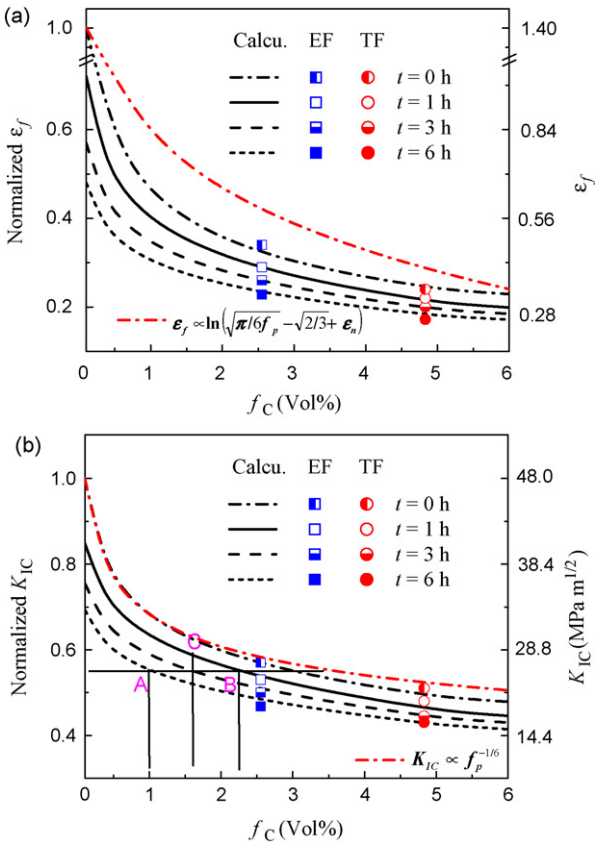

Fig. 4. Dependence of ductility ε_f (a) and fracture toughness K_{IC} (b) on the aging time (t = 0, 1, 3, 6 h) as a function of the volume fraction of the constituents. Dots are experimental results and lines are calculations. Short dot lines in (a) and (b) are from Eqs. (2) and (1), respectively, and other lines are from the multiscale fracture model.

dispersoids and precipitates as

$$\varepsilon_f = \frac{b\rho_g^c}{2\tilde{\varepsilon}_e(\theta)}\left[\frac{I}{0.405\pi h}\right]^{1/n+1}\left[\frac{\lambda_c}{2r_c}-1\right]^{1/n+1} \times(\lambda_d+\lambda_p)^{-1}\sqrt{[(1.7r_d\lambda_p)^2+(0.25\lambda_d\lambda_p)^2]}, \quad (5)$$

and

$$K_{IC} = \Gamma\sqrt{Bn^2\sigma_y\left[\frac{\lambda_c}{2r_c}-1\right]^{1/n+1}[(1.7r_d\lambda_p)^2+(0.25\lambda_p\lambda_d)^2]^{1/2}(\lambda_d+\lambda_p)^{-1}}, \quad (6)$$

with

$$\Gamma = \sqrt{\frac{CEb\rho_g^c}{2\tilde{\varepsilon}_e(\theta)}}, \quad (7)$$

and

$$B = [(1+3n)(5.39\sqrt{0.13+n}-2.53n)]^{1/n+1}, \quad (8)$$

where r_c and r_d are the radius of constituents and dispersoids ($r_d \approx 0.05\,\mu m$), λ_i ($i = c$, d, and p) is the interparticle spacing of constituents, dispersoids ($\lambda_d \approx 0.15\,\mu m$), and precipitates, respectively, $\tilde{\varepsilon}_e(\theta)$ is the effective value for normalized coefficient $\tilde{\varepsilon}_{ij}(\theta)$ and is a constant when $\theta = 0$, E and b are the elastic modulus and Burgers vector of matrix, respectively, C is a constant of ~1/40 and the critical dislocation density in the matrix, ρ_g^c, could be regarded as a constant at room temperature, n is the strain hardening exponent and I and h are functions of n [17,18]. Some parameters such as ρ_g^c and $\tilde{\varepsilon}_e(\theta)$ are difficult to determine exactly but they can be approximately regarded as constants. To overcome this problem, the strain to fracture and the fracture toughness used in this work are normalized values which are divided by a reference strain to fracture (ε_f^R) and fracture toughness (K_{IC}^R) (here the reference is chosen at the point of $f_c = 0$ and $t = 0$, where ε_f^R and K_{IC}^R are calibrated as 1.40 and 48.0 MPa $m^{1/2}$). Similar treatments have been used and addressed in previous works [12–15,19,20].

Because the parameters of precipitates are controlled by the aging treatment (Eqs. (3) and (4)), Eqs. (5) and (6) can predict the aging-modulated dependence of ductility and fracture toughness on the constituents. Calculations are shown in Fig. 4 as indicated by $t = 0$, 1, 3, and 6 h, respectively. The experimental results at different aging time are quantitatively modeled and the calculations are in good agreement with the experimental results. This indicates that the multiscale fracture model can be successfully used for evaluating the coupling effect of constituents and precipitates on the ductile fracture of heat-treatable aluminum alloys.

From Fig. 4, one can see that the EF-treated samples have ductility and fracture toughness both larger than the TF-treated samples when aged at the same t. This is because the former samples contain less brittle constituents that are usually the void/crack initiators or the preferential crack propagation path [1]. However, when aged at different t, the short-aged TF-treated samples can exhibit ductility and fracture toughness equal to or even greater than those of the long-aged EF-treated ones, e.g., the TF-treated samples aged at 1 h compared with the EF-treated samples aged at 6 h. This clearly indicates that the ductility and fracture toughness of the heat-treatable aluminum alloys are dependent not only on the μm-scaled constituents but also on the nm-scaled precipitates. It has been well known that the precipitates, blocking the move of dislocations, are apt to induce stress localization and cause the alloys readily rupture. The more and larger are the precipitates, the more intense is the stress localization. To some degrees, the influence of precipitate-induced stress localization on the ductile fracture of aluminum alloys is close to or predominant over that of the μm-scaled constituents. The EF-treated samples aged at 6 h, although having fewer constituents, contain precipitates much more and larger than in the TF-treated samples aged at 1 h. The stress localization caused by precipitates is much intense in the former samples, which will weaken the deformation capability remarkably. This can be used to well explain what mentioned above, i.e., the TF-treated sample aged at 1 h exhibits ductility and fracture toughness equal to and greater than the EF-treated samples aged at 6 h, respectively. While aged at a same t, the difference in precipitate size/content between the two treated samples is not so notable, the ductile fracture of the samples are controlled predominantly by the μm-scaled constituents. The EF-treated samples contain less constituents and so exhibit higher ductility and fracture toughness.

As to Fig. 4, it should be especially noted that, because the reference is at the point of $f_c = 0$ and $t = 0$, the calculations at $t = 1$, 3, and 6 h do not begin from 1 at $f_c = 0$. For example, calculations on ε_f begin from 0.72, 0.59, and 0.48, corresponding to $t = 1$, 3, and 6 h. In addition, the calculations from the multiscale fracture model lead to smaller values than those obtained from Eqs. (2) and (1). This is mainly due to the comprehensive consideration in the multiscale fracture model. On the other hand, only the influence of constituents is considered in Eqs. (2) and (1).

Comparing with previous works (see for example Figs. 5, 7 and 8 in Hahn and Rosenfield's review paper [1]), Fig. 4 in the present work includes more information. Firstly, the coupling effect of the constituents and precipitates (aging treatment) is clearly shown. In Fig. 4 the ductility or fracture toughness was simultaneously related to the parameters of both the constituents and the precipitates, while in most of the previous works, these properties can be only related to the parameters of one particle of either constituent or precipitate. Secondly, Fig. 4 can be used to aid the optimization of aging treatment. As seen in Fig. 4(b), although position B (~2.3%) contains more constituents than position A (~1%), the two positions can have the same level of fracture toughness (normalized $K_{IC} \approx 0.55$) after different aging treatment, i.e., 1 h for position B and 6 h for position A aged at 483 K. Thirdly, it can be also revealed from Fig. 4 that reducing the constituents content is not the only method to improve the ductility and fracture toughness of the Al alloys. For example, position C, although has more constituents (~1.5%) than position A, exhibits fracture toughness (normalized $K_{IC} \approx 0.6$) higher than that of position A. This is also caused by the appropriate choice of the aging treatment time. Using Fig. 4, it is thus possible to artificially control the aging treatment to achieve desirable properties in the present Al–Cu–Mg alloy.

4. Conclusions

The coupling effect of constituents and precipitates on the ductile fracture of Al–Cu–Mg alloy was investigated. Different solution treatments were used. Subsequently the alloy was aged to a series of times to yield various combinations of constituents and precipitates. The ductility and fracture toughness are experimentally measured and discussed with respect to the microstructural analyses. The main results are summarized as follows

(1) The EF-treated samples are found to have fewer constituents, which mean that the enhanced solution treatment is effective to reduce the constituent magnitude;
(2) The ductility and fracture toughness are dependent not only on the constituents but also on the precipitates. The short-aged TF-treated samples, although containing more constituents, can exhibit ductility and fracture toughness equal to or even greater than those of the long-aged EF-treated ones. This is because that much more precipitates in the latter samples will cause intense stress concentration and reduce the deformation capability.
(3) A multiscale fracture model was used to explain the aging-modulated influence of the constituents on the ductile fracture

and the calculations are in good agreement with the experimental results.

Acknowledgements

This work was supported by the National Basic Research Program of China (Grant No. 2004CB619303 & 2005CB623700), the National Natural Science Foundation (50701035) and the National High Technology Research and Development Program of China (2008AA031001, 2008AA031003). This work was also supported by the 111 Project of China under Grant No. B06025.

References

[1] G.T. Hahn, A.R. Rosenfield, Metall. Trans. 6A (1975) 653.
[2] G.G. Garrett, J.F. Knott, Metall. Trans. 9A (1978) 1187.
[3] J.T. Staley, Aluminum 55 (1979) 277.
[4] L.M. Brown, J.D. Embury, The microstructure and design of alloys, in: Proceedings of the Third International Conference on the Strength of Metals and Alloys, 1, The Institute of Metals, Cambridge, 1973, p. 164.
[5] S.E. Urreta, F. Louchet, A. Ghilarducci, Mater. Sci. Eng. A302 (2001) 300.
[6] T.B. Cox, J.R. Low Jr., Metall. Trans. 5 (1974) 459.
[7] R.H. Van Stone, T.B. Cox, J.R. Low Jr., J.A. Psioda, Int. Met. Rev. 30 (1985) 157.
[8] E. Hornbogen, E.A. Starke Jr., Acta Metall. 41 (1993) 1.
[9] S. Suresh, A.K. Vasudevan, M. Tosten, P.R. Howell, Acta Mater. 35 (1987) 25.
[10] D.J. Lloyd, Scripta Mater. 48 (2003) 341.
[11] D. Dumont, A. Deschamps, Y. Brechet, Acta Mater. 52 (2004) 2529.
[12] G. Liu, G.J. Zhang, X.D. Ding, J. Sun, K.H. Chen, Mater. Sci. Technol. 19 (2003) 887.
[13] G. Liu, G.J. Zhang, X.D. Ding, J. Sun, K.H. Chen, Metall. Mater. Trans. 35A (2004) 1725.
[14] G. Liu, J. Sun, C.W. Nan, K.H. Chen, Acta Metall. 53 (2005) 3459.
[15] G. Liu, G.J. Zhang, R.H. Wang, W. Hu, J. Sun, K.H. Chen, Acta Metall. 55 (2007) 273.
[16] G. Liu, G.J. Zhang, X.D. Ding, J. Sun, K.H. Chen, Mater. Sci. Eng. A344 (2003) 113.
[17] C.F. Shih, ASTM STP 560 (1974) 187.
[18] N.E. Dowling, Eng. Fract. Mech. 26 (1987) 333.
[19] S.P. Yuan, G. Liu, R.H. Wang, X. Pu, G.J. Zhang, J. Sun, K.H. Chen, Scripta Mater. 57 (2007) 865.
[20] S.P. Yuan, G. Liu, R.H. Wang, G.J. Zhang, X. Pu, J. Sun, K.H. Chen, Mater. Sci. Eng. A 499 (2009) 387.